A Hybrid Ray-Wave Optics Model to Study the Scattering Behavior of Silver Metallic Paint Systems

C.M. SEUBERT[1, 2*], M.E. NICHOLS[1], C. KAPPAUF[1], K. ELLWOOD[1], M. SHTEIN[2] and M.D. THOULESS[2, 3]

[1]*Materials Research Department, Ford Motor Company, Dearborn, MI 48124, USA*
[2]*Department of Materials Science & Engineering, University of Michigan, Ann Arbor, MI 48109-2125, USA*
[3]*Department of Mechanical Engineering, University of Michigan, Ann Arbor, MI 48109-2125, USA*
[*]*Primary author contact: cseubert@ford.com, 313-322-3070*

Abstract

The gonioapparent lightness of a metallic paint system depends strongly on the 3D microstructure of the platelet-containing basecoat layer, and on the platelet roughness. Current optical models used to simulate the paint's appearance, however, ignore the multi-scale and multi-dimensional microstructural features, which limits their predictive power. Here, we describe a hybrid, ray-wave optics model for metallic paints. This model incorporates the ray optics of the 3D platelet microstructure, and the wave effects that result from the surface roughness of the platelets. This model is used to link the roughness to the reflection lobes of the aluminum platelets, and to the gonioapparent lightness of the paint system. Predicted lightness values from our model matched, at most viewing angles, measurements from physical paint samples. This model can be used to explore the effect of platelet surface roughness on the lightness of the complete paint system, and predict the appearance of paints with different platelet microstructures.

1. Introduction

It is important for industries that manufacture consumer products to understand how customers perceive color, and how specific colors are physically produced. One class of colors desired by designers and customers are gonioapparent colors; i.e. those that change appearance with variations in angle of illumination and/or observation [1]. These colors are quantified using parameters such as lightness (L^*), chroma, and hue [2–5], which are controlled by the incorporation of pigments and/or high-aspect ratio platelets into the color layer of a paint system. The metallic platelets act as microscopic mirrors, and provide a strong specular component to the light reflected from the paint's surface.

The design and manufacturing processes could be accelerated and enhanced substantially if the appearance of color can be predicted prior to part production. Ideally, designers and engineers could use such a method to visualize a new color that optimizes specific properties such as, lightness, chroma, hiding, or cost. They could also assess the risk of unacceptable color harmony (match) on objects painted with highly gonioapparent colors. This assessment is important for quality control, as changes in the appearance as a function of observation angle are often mistaken for poor color harmony on geometrically complex objects.

To model or quantify the color and appearance of an object, the object's light-scattering behavior can be described by the bidirectional reflection distribution function (BRDF) [6], which is commonly estimated from measurements of small sub-sections of the full scattering function. Simple, diffuse-color systems were first modeled by Kubelka and Munk [7], and Saunderson [8]. These models have been incorporated into modern graphical-rendering systems, and provide a

realistic, if not exact, match between the appearance of rendered objects and physical samples [9–12]. Previous work has shown that using just three angles of observation suffices to model the full BRDF for *simple* colors [13,14], but can lead to inaccurate predictions of color shifts with angle for *gonioapparent* colors [15].

While significant progress has been made to render colors accurately using complete or partial BRDF scans, predictive modeling of colors from material and microstructural data lags in development. Attempts have been made to predict the appearance of multilayered paint systems by combining the measured scattering behavior of the individual layers into a single, bulk scatterer [16–18]. In addition, researchers have used microfacet models to simulate the appearance of metallic paint [17,19,20], assuming a single metallic surface with facets at different orientations, each reflecting light in a specular fashion. However, neither of these techniques accounts for edge effects and gaps between the platelets or the surface roughness of the platelets/facets.

The modeling of a complete 3D microstructure would improve our ability to predict the scattering behavior of a paint system containing layered platelets. However, while a great deal of work has been conducted on the scattering of radiation and light from individual, rough metallic surfaces [21–27], no work has been done to examine how the presence of such rough scatterers would affect the gonioapparent behavior of platelet-containing coatings. The assumption of specularly reflecting platelets limits the accuracy of pure ray-based models, but no model with rough surfaces has been created to predict paint appearance. We address this issue in the current study by creating an accurate, hybrid ray-wave model to predict the

scattering behavior of a metallic-paint system. A flow diagram depicting the process used to simulate the appearance of the material is shown in **Figure 1.**

The model was validated using two metallic-paint samples with qualitatively different

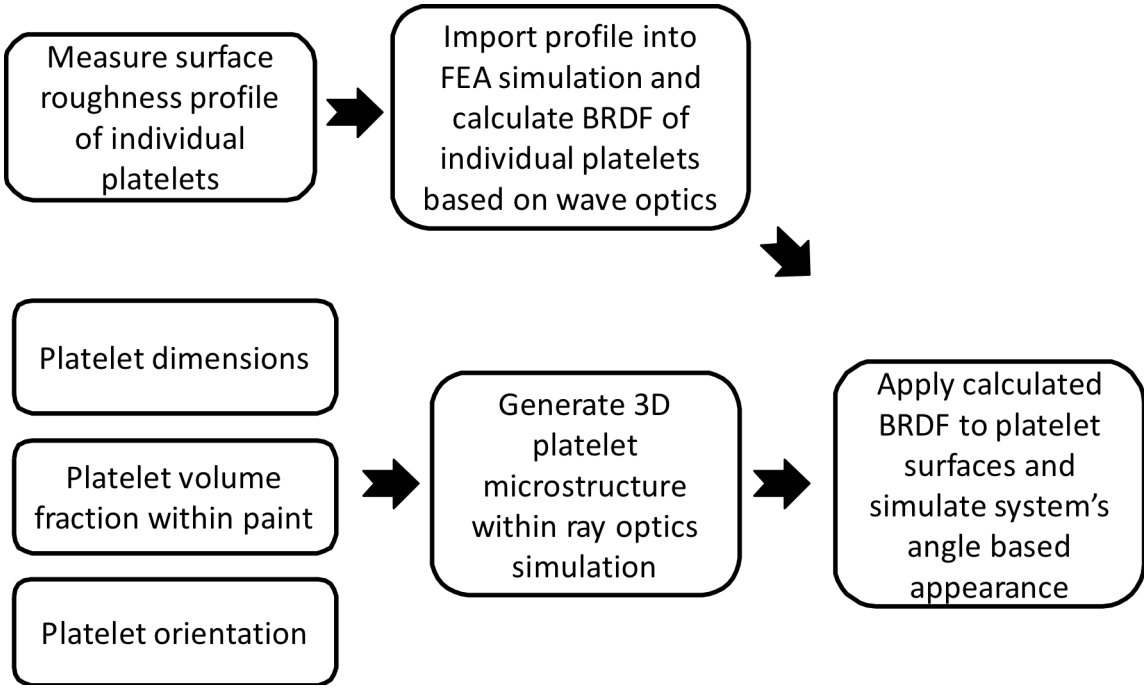

Figure 1: Flow diagram illustrating the process used to create the hybrid ray-wave model and to calculate the angle-based appearance of the material.

platelet orientations. The appropriate roughness values and the characteristics of the platelet arrays were obtained from experimental measurements, and the parameters incorporated into the models. The resultant predictions of the appearance were then compared directly to spectrophotometer measurements of the physical samples.

2. Background

The appearance of a surface can depend on both the angle of incidence and the angle of observation. When light hits a surface it can be reflected or scattered in different directions. There are two limits for the reflection of a light ray. In one limit, the ray is reflected in a specular fashion, as from a mirror, with the angle of reflection equal to the angle of incidence. In the other limit, a light ray is scattered uniformly in a diffuse fashion at all angles. Generally, the behavior lies somewhere in between these two limits, and the reflection is described by what is known as a bidirectional reflection distribution function (BRDF) **(Figure 2)** [6].

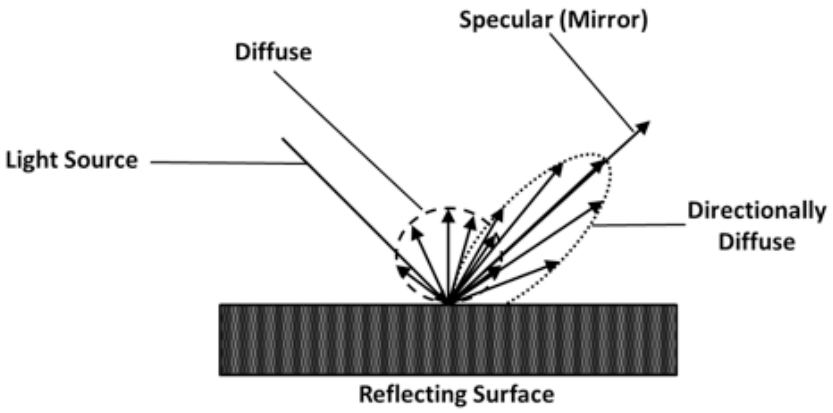

Figure 2: 2D schematic of different BRDFs that result from perfectly specular, directionally diffuse, and diffuse surfaces.

2.1 Pigments and Paint

A schematic of a typical automotive paint system is shown in **Figure 3**. Many paint systems are multi-layered materials that possess a color layer called the "basecoat". Pigments, platelets, and other scatterers are added to the basecoat layer to impart a specific color [28–30]. Many paints, particularly those whose pigment particles have shapes with an aspect ratio near one, and are opaque, exhibit little variation in appearance with illumination or observation

angle. On the other hand, metallic paints contain aluminum platelets that produce a gonioapparent behavior [31], in which the appearance does depend on the angle of illumination or observation. In particular, the paint system considered in this paper is a very common "special effect" option used by designers, with a look characterized by a "salt and pepper" texture, as well as the lightness changes associated with gonioapparent behavior [31,32].

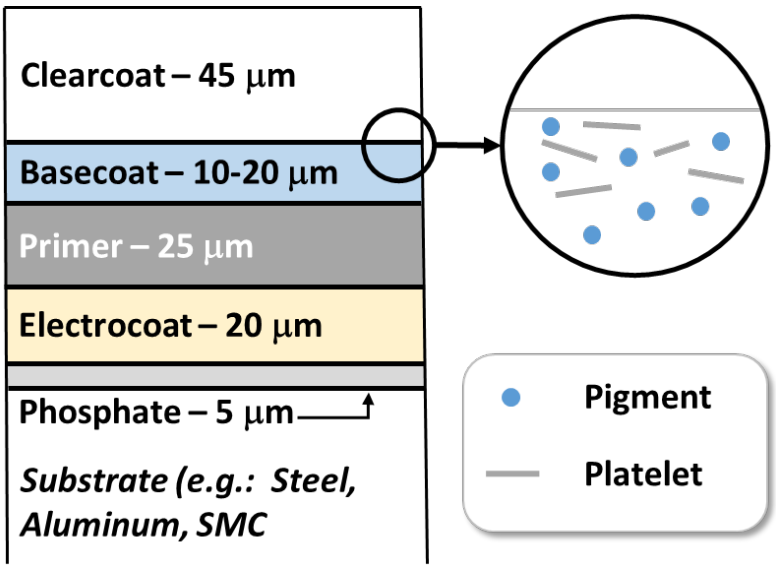

Figure 3: Schematic illustration of a typical automotive paint system. There can be pigments and / or platelets contained within the basecoat layer. These act as scatterers to provide the desired color and appearance of the paint system.

It has been shown that the microstructure of the paint, the size of the platelets (width and thickness), the pigment volume concentration (PVC) of platelets, and the orientation of the platelets in the coating, affect the appearance of the paint system [31, 32,33,34]. However, the surface roughness of the platelets can also affect the overall appearance. As such, surface

roughness must be incorporated into any model that attempts to accurately predict the appearance of a metallic paint system. A simple scattering term cannot be added to the system as a whole, since differences in platelet orientation can mask the effect of platelet surface roughness on the BRDF of the entire paint system [35].

2.2 Scattering of light from a rough metal surface

The BRDF of a metal surface is directly affected by its roughness [17, 19-23]. While the simplest way to quantify these effects is to measure the BRDF directly, it is not always possible to conduct a physical measurement because of size and time constraints, the lack of physical samples, or the fragility of a physical sample. In these cases, reflection models have been proposed by a number of researchers to predict the BRDF of a roughened metallic surface [36–43]. These models are based on two key surface-roughness parameters, the root-mean square (RMS) roughness (σ_{RMS}) and the correlation length (τ).

One of the most accurate models used for reflection in computer graphics is the He-Torrance model [36]. This model uses the Kirchhoff approximation, where fields at any point on the surface are approximated by fields on an extended tangential plane [44,45], combined with additional shadowing and geometric components [36]. However, it is too computationally complex for use in routine rendering applications, and computationally cheaper models are preferred.

More generally, and for accurate predictions without the approximations inherent in the He-Torrance model, one can integrate Maxwell's equations for a roughened surface. Unlike the He-Torrance model, this can be done for any magnitude of σ_{RMS}, τ, angle of incidence (θ), and

wavelength (λ). Until recently, this has not been possible because of computational limitations. New finite-element analysis (FEA) tools, and improved computer hardware, have made it possible to predict the scattering from rough surfaces at a small scale [46–48]. Isakson modeled scattering behavior of the ocean floor and found that the FEA method produced similar results to the Kirchhoff and small perturbation approximations in their regions of validity, and matched the exact integral solution in all cases [48]. This shows that it may be possible to use FEA to model the effect of surface roughness on the scattering behavior of individual platelets and, hence, of the entire paint system. In particular, real-time rendering is not needed for the purposes of this study, making the integration and solution of Maxwell's equations for a particular scattering surface even more feasible.

2.3 Digital Modeling of Paint Systems

To address the limitations of previous models that were discussed previously, we use a hybrid ray-wave optics approach [49] to assess the interaction of light with the entire microstructure. Ray casting allows us to quantify the effect of platelet-to-platelet multiple-scattering events that occur within the 3D microstructure of the paint system. Each reflection from the surface of a platelet will follow a prescribed BRDF that will be calculated from wave-optics simulations for rough surfaces. It is this hybrid ray-wave approach that we feel can be used to predict the scattering and lightness behavior of these metallic coatings more accurately than other models.

3. Materials and methods

3.1 Paint materials and application

The physical samples used in this study consisted of a standard, silver, metallic automotive basecoat/clearcoat paint system. The PVC of the basecoat in each sample was 20% ± 1%. The paint system was sprayed to hiding (~20 μm) [50] with a rotary bell applicator onto steel panels that had been previously coated with a grey automotive primer. Low-fluid-flow and high-fluid-flow bell-application processes were used to produce two physical samples: one with platelets more highly oriented (Silver #1) than the other (Silver #2). The basecoat was allowed to flash dry at ambient temperature before application of the clearcoat. The target thickness of the fully cured clearcoat layer was 50 μm, and the clearcoat was also flash dried at ambient conditions to allow for solvent evaporation. The samples were cured in a convection oven for 20 minutes at 130^{o}C.

3.2 Experimental methods

3.2.1 Platelet extraction and optical profilometry

A portion of wet basecoat was diluted with methylene chloride, and vacuum filtered through Grade-2 filter paper to create a layer of platelets on the surface of the filter paper. After the initial filtration step, additional methylene chloride was sprayed onto the filtered platelets to ensure that any residual acrylic binder was removed. Individual platelets were isolated from the layer left on the filter paper, and the surface topographies of 10 individual aluminum platelets from the paint systems were characterized using a Wyko NT3300 (Bruker Corp., Billerica, MA), non-contacting, white-light interferometer (**Figure 4**). Single line scans of

the surface profiles over the full length of each of these platelet (10-30 μm), were then extracted from these profiles. A Gaussian filter with a cutoff of 50% the scan length was used to remove the curvature from the scans, and the end-points of each scan were used for leveling. σ_{RMS} = 51 nm ± 10 nm was calculated as the root-mean-square average of the peak-to-valley heights; τ = 640 nm ± 110 nm was identified as the shortest in-plane distance over which the autocorrelation function decayed to 1/*e* or ~0.37.

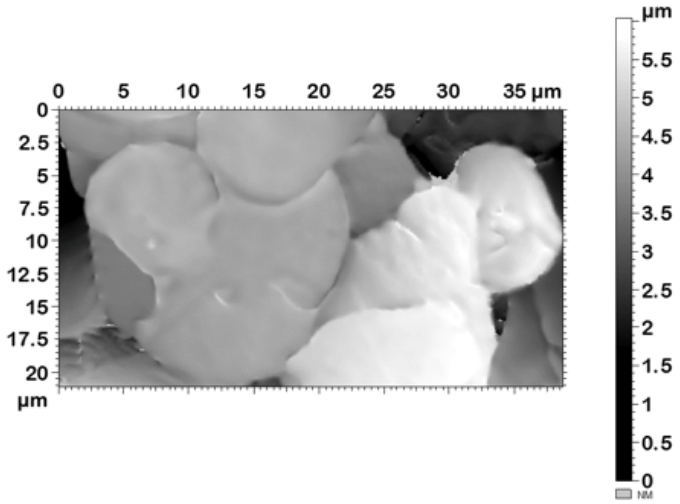

Figure 4: Optical profilometry scan of platelets extracted from silver metallic paint system. Flakes were washed in acetone and vacuum filtered through No. 2 filter paper.

3.2.2 Microstructure

The orientation distribution and the characteristic dimensions of the platelets in the two paint systems had been determined using laser-based confocal microscopy in an earlier study [51]. These systems were identified as Silver #1 and Silver #2 in that study, with the dimensions

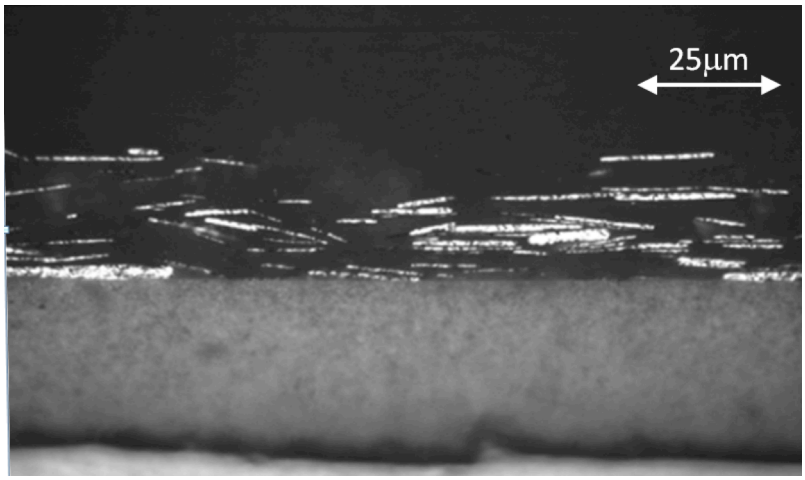

Figure 5: 2D cross sectional view of Silver #1 that was studied previously [51]. Area fraction of the platelets was measured for a series of cross sections to determine the approximate volume concentration of a typical hiding silver basecoat. This pigment volume concentration was calculated to be 20 ± 4%.

being given in Table 1 of Ref. [51] and the orientation distributions being given in Fig. 7 of that reference. The best description for the measured orientation distributions was found to be 2-parameter gamma functions. The shape and scale parameters for these gamma function were 2.29 ± 0.05 and 2.18 ± 0.03, for Silver #1, and 2.98 ± 0.07 and 2.10 ± 0.03, for Silver #2. The volume concentration of the pigments had been determined from cross-sectional microscopy in the earlier study to be 20 ± 4 % (see **Figure 5**) [51]. The size distribution of the platelets had been determined from the confocal microscopy scans taken in the earlier study, and fitted to a 9^{th} degree polynomial [51]. The values for the thickness of the platelets were obtained from the pigment supplier.

3.3 Simulation methods

3.3.1 Finite-element simulations of surface scattering

The effect of surface roughness on the BRDF of an aluminum platelet was calculated using FEA software (Comsol Multiphysics Comsol, Inc., Burlington, MA). 2-D surface scans (20 μm in length) of the platelets were imported from the optical profilometry measurements (schematic shown in **Figure 6)**. To reduce computational complexity, the scattering simulations were carried out in two dimensions, and the platelets were assumed to have a BRDF that was axisymmetric about the normal.

The aluminum was assigned an impedance boundary condition because its skin depth at visible wavelengths is very small (~3 nm). Skin depth is a measure of how deeply electromagnetic waves penetrate into a material [52], and is dependent on the material properties and the frequency of the incident radiation. Most metals have a very small skin depth at visible wavelengths [53].

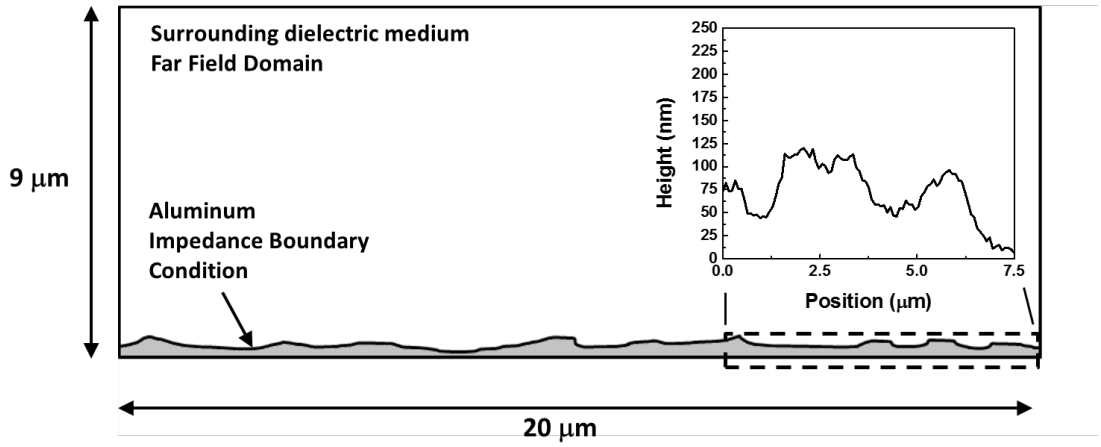

Figure 6: FEA simulation setup consisting of an single aluminum platelet and surrounding dielectric medium. An impedance boundary condition was used for the surface of the aluminum due to the small skin depth and to reduce the simulation size. The 2-D line scan obtained from the optical profilometry was imported and used to create the aluminum boundary. The callout is a plot of an actual 2-D line scan from a platelet from Silver #1.

It was assumed that there was a 9 μm thick dielectric medium above the aluminum surface. The index of refraction (*IOR*) for this medium was taken to be 1.5 [54], which is the approximate value for an acrylic resin. The three boundaries of the dielectric region were designated as scattering boundary conditions with perfect transparency to scattered waves. This dielectric region was also designated as the far-field domain to capture the shape of the far-field scattering pattern. The background electric field present in this dielectric region was assumed to have a wavelength of 500 nm, and the light was assumed to be at a normal angle of incidence, so as to generate a symmetric scattering lobe.

The resulting scattering data were imported into a commercial ray-optics software package (TracePro, Lambda Research Corp, Littleton, MA, USA), and converted into surface BRDFs for the platelets. The conversion process assumed scattering was symmetrical about the scattering plane, and adjusted the shape of the reflection lobe to account for different angles of

incidence. The results from all the different simulations were combined to give an average BRDF that was used in the subsequent simulations.

3.3.2 Creation of a platelet array

A 3D platelet array was created *in silico* to model the complete microstructure of the silver metallic-paint system. This array incorporated not only the platelets at the surface of the basecoat layer, but also the platelets contained throughout the basecoat thickness. The platelets were assumed to be rectangular prisms with equal sides, having a thickness and distribution of orientations based on measurements taken from the physical samples in our previous study [51]. The orientation distributions were used to assign a rotation to each of the simulated platelets. Each platelet was assigned the BRDF that had been computed as described above. In addition, the attenuation caused by reflection from the aluminum platelets was fixed at ~8%: an appropriate value for the wavelength of light used in the simulation [55].

Two additional assumptions were made in the creation of the simulated array of platelets. First, each platelet was randomly rotated about the axis normal to the paint system [50]. Second, the platelets were randomly distributed within the volume of the platelet-containing layer, with no preferential layering or structure [56]. These assumptions reduced the computational complexity of the platelet generating/placement algorithm.

The platelets were assumed to have a fixed thickness of 1 μm. Their center points were randomly assigned a location, and their width determined from the ninth-order polynomial that had been used to fit the measured cumulative-distribution function of their size. The random placement of platelets resulted in multiple platelets occupying the same physical space.

Therefore, a piercing-check algorithm based on an intersecting triangle algorithm developed by Moller [57], with some modifications, was implemented to minimize this issue. The geometry of each platelet was incorporated into the algorithm, with the mid-plane of each platelet being subdivided into four triangular regions. The mid-plane was selected to reduce the number of surfaces checked for intersection, reducing computing cost. Triangles in platelets that were close to each other were then checked for intersection. Intersecting platelets were assigned a new location, while maintaining their orientation and size. This replacement continued until either no intersections were detected, or 1000 failed attempts had been made (to reduce computational time). Note that there could still be piercings at the true simulated platelet surfaces, which are offset from the mid-plane. However, the offset distance was small enough to allow the assumption that the number of missed intersections was small, producing a negligible effect.

3.3.3. Creation of paint system

Using the approach described above, a platelet array of 15 x 20 mm was created. Its size was designed to exceed the illuminated area. Once built, the model of the platelet array was imported into the ray-tracing environment, and surrounded by a volume of material with an index of refraction of 1.5 [54]. A platelet-free clearcoat, with a thickness of 50 μm, was put on top of the simulated basecoat, with no unique optical interface between the two layers. The lack of an optical interface is consistent with the automotive industry standard practice of wet-on-wet application of the basecoat and clearcoat layers, where intermixing between the layers occurs during application and cure.

This model was then used in a commercial ray-optics package (TracePro, Lambda Research Corp, Littleton, MA, USA). The ray-trace simulations assumed a collimated light source consisting of 5M individual rays randomly distributed across the aperture, with each ray assigned a flux of 1 watt and a wavelength of 546 nm. The flux of each ray was not significant, as *L** calculations were performed on a relative scale. The wavelength of the light source was also not significant because aluminum platelets reflect uniformly across the visible spectrum, and no other absorptive species are present within these simulated systems. The reflection of a ray at platelet was determined by the BRDF calculated for the platelets.

The results of the simulation were then compared to lightness measurements of the two physical samples under study. These measurements were made using an MA98 handheld spectrophotometer (X-rite, Inc., Grand Rapids, MI, USA). Since handheld spectrophotometers measure a small subset of the BRDF, and report lightness values at prescribed angles of illumination and observation, a similar virtual device was built within the simulation environment.

4. Results

4.1 Optical profilometry and simulated BRDF of platelets

An example of a line scan taken from the surface profile of a platelet is shown in **Figure 7**. The line scans from the 10 extracted platelets were then imported into the FEA simulations used to calculate the BRDFs. These BRDFs were then combined into a single effective function, shown in **Figure 8**. It will be seen that this BRDF possesses a clear specular peak, but also contains a significant amount of light outside the specular zone.

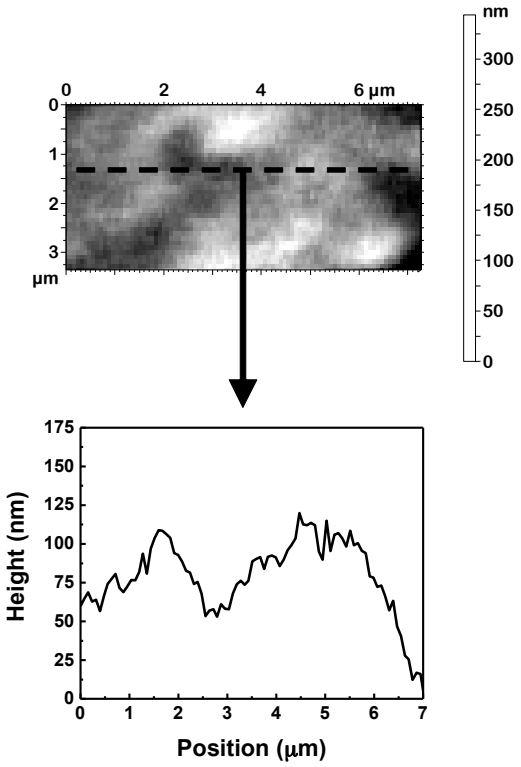

Figure 7: An example of a line profile extracted from a scanned platelet from Silver #1. A series of these line profiles were used in the FEA simulations to generate the BRDF of each line profile.

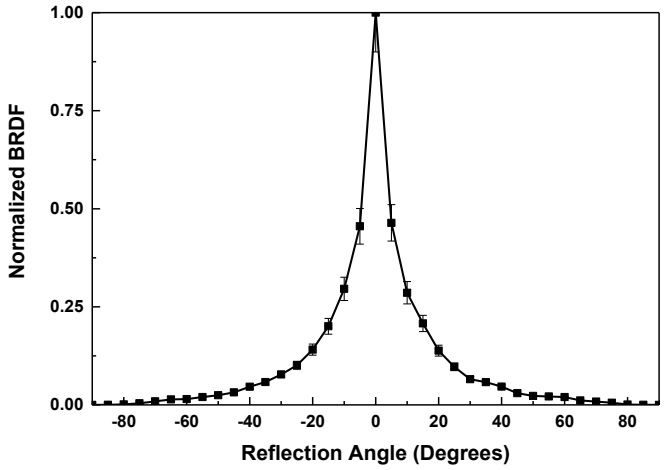

Figure 8: Average BRDF normalized to a maximum reflectivity of 1.00, obtained from FEA simulations for ten extracted aluminum platelets. Angle of incidence was normal to the surface. The reflection pattern still contains a strong specular peak, but contains light outside of the specular zone. The line connecting the data points is a visual guide only.

4.2 Five angle lightness values of ray trace simulations and physical measurements

The lightness values (*L**) for each of the two physical samples under examination were measured using a handheld spectrophotometer, and are reported in **Table 1**. The hybrid simulations allowed *L** to be calculated at the same standard five angles of observations: 15^{o}, 25^{o}, 45^{o}, 75^{o}, and 110^{o}. The difference between the simulated values of *L** and the physically measured values at each of the five angles of observation are listed in **Table 1** for both Silver #1 and Silver #2.

The results of a microfacet simulation (no gaps, 3D microstructure, and no surface roughness assigned to the platelets) are also shown in **Table 1.** These are based on the same measured platelet orientations, but with an assumption of purely specular reflection from the platelets. It will be seen that the hybrid ray-wave model results in a relatively accurate simulation of *L** at 15^{o}, 25^{o}, 75^{o} and 110^{o} when compared to the physical measurements, and provides a dramatic improvement over the specular microfacet model. However, the difference between the hybrid simulation and the physically measured values of *L** at 45^{o} is large, with the simulations predicting a significantly lighter sample than physically observed. This discrepancy is discussed in the next section.

Table 1: Lightness for each of the physically measured and simulated samples. The difference between the simulated and physically measured samples varies based on the angle of observation. The simulation matched well at all angles of observation except 45° OS.

Sample Name	Physical/ Simulation	Platelet BRDF Shape	L^*_{15}	L^*_{25}	L^*_{45}	L^*_{75}	L^*_{110}
Silver #1	Physical	N/A	143.3± 0.3	107.2± 0.3	58.6 ± 0.3	37.2± 0.3	32.1± 0.3
Silver #1	Hybrid Simulation	Measured	128.2± 0.5	112.6± 1.2	81.3± 2.1	42.1± 0.7	36.3± 0.8
Silver #1	Microfacet Simulation	Specular	187.5± 0.7	128.6± 0.5	50.6± 0.2	4.2± 0.02	0
Silver #2	Physical	N/A	129.0± 0.3	106.1± 0.3	67.7± 0.3	43.7± 0.3	36.2± 0.3
Silver #2	Hybrid Simulation	Measured	122.9± 0.5	109.5± 1.2	81.6± 2.1	47.1± 0.7	37.0± 0.8

5. Discussion

5.1 *FEA simulation compared to He-Torrance*

Within the limits where its approximations are valid, the He-Torrance model of reflection [36] is considered to be the best currently available. While our FEA simulations are not subject to the same length-scale limitations and approximations as the He-Torrance model, because the FEA model uses real surface profiles, it is instructive to compare the results from the two methods.

A BRDF was created from an artificially generated Gaussian surface with roughness parameters similar to the aluminum material modeled by He. This surface was created within MATLAB (MathWorks, Natick, MA, USA), using code based on work by Bergström et al. [58] and Garcia & Stoll [59] and roughness parameters of σ_{RMS} = 280 nm and τ = 1770 nm. The surface was illuminated at an angle of 10° following Ref. [36] A BRDF was generated for this surface

using the approach described in Section 3.3.1. The resultant BRDF was then compared to that obtained in Ref. [36].

Figure 9 shows a comparison between the He-Torrance model, measurements taken from a physical sample in Ref. [36], and the results generated by the FEA technique presented here. It will be observed that the results from the FEA technique match those of the He-Torrance model across the entire reflection pattern, with both models deviating from the physical measured sample at large reflection angles. This deviation may be caused by the imperfect nature of platelet edge surfaces that occur on physical samples, but it is not explicitly taken into account in our current model or in the He-Torrance model. This could lead to visual discrepancies between physical and digital samples based on these models when an object is viewed at these large reflection angles.

It should be noted that the size of the FEA simulation might need to be altered if it is to be used for significantly longer/shorter wavelength and surface roughness scales. Examples include radar and microwave scattering from large surfaces. While the FEA technique does not include any length-scale assumptions like the He-Torrance and other reflection models, it does require a simulation geometry that is sufficiently large to capture a statistically representative interaction of light with the surface.

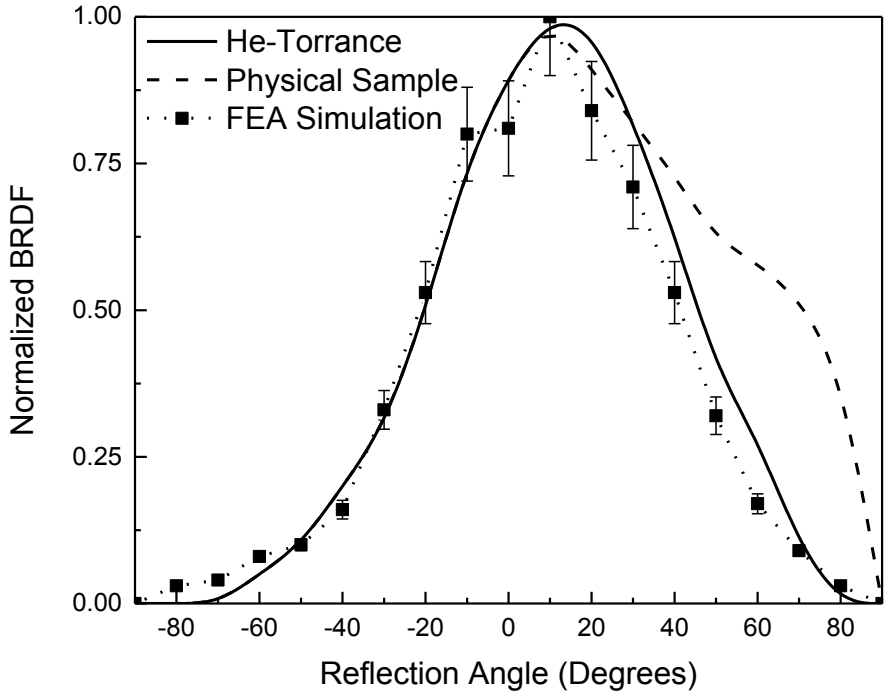

Figure 9: Plots of the normalized BRDF reflection lobe for an aluminum surface with σ_{RMS} = 280 nm and τ = 1770 nm, wavelength of 500 nm, and a 10^{o} angle of incidence. There is good agreement between the results based on (i) the He-Torrance model [35], (ii) experimental data taken from Ref. [36], and (iii) the FEA simulation presented in this paper.

5.2 Comparison between simulated lightness values and physical measurements

The comparisons between the values of *L** obtained from simulations and the corresponding measured values are shown in **Table 1**. The biggest difference between the simulated results and the observed measurements is a 15-20-point difference in lightness at 45^{o}. The waviness of the surface of the clearcoat, which can have a σ_{RMS} greater than 200 nm, was not considered in the simulations. This waviness may reduce the lightness at 45^{o} by scattering light away from the normal direction, owing to refraction at the surface of the clearcoat. While this waviness does not appear to provide an effect great enough to cause any

obvious haze or reduction in distinctness of image, it should be examined in future versions of the model to identify if it does indeed affect some observation angles more than others do.

While there are some discrepancies in the details of how well the simulations match experimental results, the major observation of the results given in Table 1 are that simulations incorporating the roughness of the platelets are more accurate than simple, specular microfacet models. For example, they allowed us to capture the darkening at 15^{o} and the lightening at 110^{o} that was observed in the physical samples, but missed in the microfacet model. This nuanced color behavior is critical to designers who have been hesitant to make design decisions digitally because of the deviations between models and their specific colorimetric targets. The proposed hybrid ray-wave model allows one to identify meaningful differences in lightness that result from microstructural changes to the platelet layer of the paint system.

6. Conclusion

Metallic- paint systems contain features on a variety of size scales, from micrometer-sized platelets arranged in multiple layers to the nanometer-sized roughness of the platelet surfaces. These multiple length scales were the motivation to use a hybrid approach that incorporated both wave and ray optics within a single simulation environment. This sequential, hybrid approach was used to predict the scattering behavior of silver metallic-paint systems, and to predict how the platelet microstructure and the surface roughness affect the appearance of the system. The approach was more accurate than a microfacet model of the

same system. Moreover, the approach can be used to predict the scattering behavior of any 3D layered structure without the limitations of scale imposed by other models.

Color and appearance is a key product differentiator for a range of industries. The hybrid modeling approach presented in this paper can be used to minimize the time and cost associated with the development of a new color. The method has the ability not only to improve the efficiency of current color development processes, but also to create and simulate precise, highly customized platelet microstructures. This ability could be used to help guide future manufacturing advancements that focus the physical creation of such precise microstructures, be it for paints, plastics, cosmetics, or other decorative materials.

This hybrid approach can be used to model the impact of unique scattering media contained within a dielectric medium. Particles or platelets based on structural color, interference effects, or other unique scattering or absorptive properties can be built into a model paint system and optically analyzed. The use of this model can help designers and engineers focus their development efforts on high impact, high return systems that provide new and unique appearance characteristics.

Other areas where this approach might prove useful is in the creation of stealth and cloaking technologies. Physical prototypes of these technologies are difficult and expensive to produce. The approach presented in this paper could be used to evaluate new scattering technologies, and to identify potential systems and microstructures of interest. Once these technologies have been placed into a digital-simulation environment and optimized, physical

samples could be produced and tested for performance to minimize the cost and development time.

References

1. Leloup F, Hanselaer P, Pointer MR, Versluys J (2005) Characterization of gonio-apparent colours. 10th AIC Congress Granada Proceedings 1:515-518.
2. Schanda J (2007) Colorimetry: Understanding the CIE system. John Wiley & Sons, Hoboken.
3. McLaren K (1976) XIII—The development of the CIE 1976 (L* a* b*) uniform colour space and colour-difference formula. Journal of the Society of Dyers and Colourists. 92:338-341.
4. Robertson AR (1990) Historical development of CIE recommended color difference equations. Color Research & Application 15:167-170.
5. Wyszecki G, Stiles WS (1982) Color science. Wiley, New York.
6. Bartell FO, Dereniak EL, and Wolfe WL (1981) The theory and measurement of bidirectional reflectance distribution function (BRDF) and bidirectional transmittance distribution function (BTDF). In 1980 Huntsville Technical Symposium. International Society for Optics and Photonics 154-160.
7. Kubelka P, Munk F (1931) An article on optics of paint layers. Z. Tech. Phys 12:593-601.
8. Saunderson JL (1942) Calculation of the color of pigmented plastics. JOSA 32:727-729.
9. Abdul-Rahman A, Chen M (2005) Spectral Volume Rendering based on the Kubelka-Munk Theory. Computer Graphics Forum 24:413-422.
10. Lei SIE, Chang CF (2005) Real-time rendering of watercolor effects for virtual environments. Advances in Multimedia Information Processing-PCM 2004, Springer, Berlin, 474-481.
11. Huang CG, Huang TS, Lin WC, Chuang JH (2013). Physically based cosmetic rendering. Computer Animation and Virtual Worlds 24: 275-283.
12. D'Eon E, Luebke D, Enderton E (2007) Efficient rendering of human skin. Proceedings of the 18th Eurographics conference on Rendering Techniques Eurographics Association, 147-157.
13. Alman DH (1987) Directional color measurement of metallic flake finishes. Proceedings of the ISCC Williamsburg Conference on Appearance.
14. Rodrigues ABJ (1990) Measurement of metallic and pearlescent finishes. Die Farbe, 37:65-78.
15. Bärz J, Henrich N, Müller S (2010) Validating Photometric and Colorimetric Consistency of Physically-Based Image Synthesis. Conference on Colour in Graphics, Imaging, and Vision, Society for Imaging Science and Technology, 148-154.
16. Ershov S, Kolchin K, Myszkowski K (2001) Rendering Pearlescent Appearance Based On

Paint-Composition Modelling. EUROGRAPHICS 2001, 20:227-238.
17. Weidlich A, Wilkie A (2007) Arbitrarily layered micro-facet surfaces. Proceedings of the 5th international conference on Computer graphics and interactive techniques in Australia and Southeast Asia. ACM 1:171-178.
18. Seo MK, Kim KY, Kim DB, Lee KH (2011) Efficient representation of bidirectional reflectance distribution functions for metallic paints considering manufacturing parameters. Optical Engineering, 50:013603.
19. Ashikmin M, Premoze S, Shirley P (2000) A microfacet-based BRDF generator. Proceedings of the 27th annual conference on Computer graphics and interactive techniques. ACM Press/Addison-Wesley Publishing Co. 65-74.
20. Jakob W, Hasan M, Yan LQ, Lawrence J, Ramamoorth R, Marschner S (2014) Discrete stochastic microfacet models. ACM Transactions on Graphics (TOG), 33:115.
21. An KH, O'Connor B, Pipe KP, and Shtein M, (2009) Organic photodetector with spectral response tunable across the visible spectrum by means of internal optical microcavity. Organic Electronics, 10(6), 1152-1157.
22. Beaglehole D and Hunderi O (1970) Study of the interaction of light with rough metal surfaces. I. Experiment. Physical Review B 2(2): 309-321.
23. Celli V, Maradudin AA, Marvin AM, and McGurn AR (1985) Some aspects of light scattering from a randomly rough metal surface. J. Opt. Soc. Am. A. 2:2225-2239.
24. Bennett HE and Porteus JO (1961) Relation between surface roughness and specular reflectance at normal Incidence. J. Opt. Soc. Am. 51, 123-129.
25. Birkebak RC and Eckert EG. (1965) Effects of roughness of metal surfaces on angular distribution of monochromatic reflected radiation. ASME. J. Heat Transfer. 87(1):85-93.
26. Peiponen KE and Tsuboi T (1990) Metal surface roughness and optical reflectance. Optics & Laser Technology. 22(2):127-130.
27. Hongsong L and Torrance KE (2005) An experimental study of the correlation between surface roughness and light scattering for rough metallic surfaces. Proc. SPIE 5878, Advanced Characterization Techniques for Optics, Semiconductors, and Nanotechnologies II, 58780V.
28. Lambourne R, Strivens T (1999) Paint and surface coatings: theory and practice. Elsevier, West Sussex.
29. Levinson R, Berdahl P, Akbari H (2005) Solar spectral optical properties of pigments—Part I: model for deriving scattering and absorption coefficients from transmittance and reflectance measurements. Solar Energy Mater Solar Cells 89:319-349.
30. Gunde MK and Orel ZC (2000) Absorption and scattering of light by pigment particles in solar-absorbing paints. Appl Opt. 39:622-628.
31. McCamy C (1996) Observation and measurement of the appearance of metallic materials. Part I. Macro appearance. Color Research & Application 21:292-304.
32. Kirchner E, van den Kieboom GJ, Njo L, Super R, Gottenbos R (2007) Observation of visual texture of metallic and pearlescent materials. Color Research & Application. 32:256-266.
33. Maile FJ, Pfaff G, Reynders P (2005) Effect pigments—past, present and future. Progress in Organic Coatings 54:150-163.

34. Pfaff, G. (2001) Special Effect Pigments. High Performance Pigments (ed H. M. Smith), Wiley-VCH Verlag GmbH & Co. KGaA, Weinheim, FRG.
35. Ellwood KR, Tardiff JL, Alaie SM (2014) A simplified analysis method for correlating rotary atomizer performance on droplet size and coating appearance. Journal of Coatings Technology and Research 11:303-309.
36. He XD, Torrance KE, Sillion FX, Greenberg DP (1991) A comprehensive physical model for light reflection. SIGGRAPH Comput. Graph. 25(4):175-186.
37. Cook RL and Torrance KE (1982) A Reflectance Model for Computer Graphics. ACM Trans. Graph. 1:7-24.
38. Smith B (1967) Geometrical shadowing of a random rough surface. IEEE Transactions on Antennas and Propagation. 15(5):668-671.
39. Barrick D (1968) Rough Surface Scattering Based on the Specular Point Theory. IEEE Transactions on Antennas and Propagation. 16(4):449-454.
40. Tang K and Buckius RO (2001) A statistical model of wave scattering from random rough surfaces. International Journal of Heat and Mass Transfer. 44(21):4059-4073.
41. Hunderi O and Beaglehole D (1970) Study of the interaction of light with rough metal surfaces. II. Theory. Physical Review B. 2(2): 321-329.
42. Garcia N and Stoll E (1984) Monte Carlo calculation for electromagnetic-wave scattering from random rough surfaces. Physical review letters. 52(20): 1798-1801.
43. Bendler JT, Feldman SF, Hatti H, Hobbs SY (1998) Approximate model of diffuse reflectance from rough polymer surfaces. Journal of applied physics. 83(2):998-1004.
44 . Chen MF and Fung AK (1988) A numerical study of the regions of validity of the Kirchhoff and small-perturbation rough surface scattering models. Radio Science. 23(2):163-170.
45 . Beckmann P, Spizzichino A (1987) The scattering of electromagnetic waves from rough surfaces. Artech House, Inc., Norwood.
46. Bonomo AL, Isakson MJ, Chotiros NP (2014) Acoustic scattering from a sand layer and rock substrate with rough interfaces using the finite element method. The Journal of the Acoustical Society of America. 135(4):2298-2298.
47. Bonomo AL, Isakson MJ, Chotiros NP (2015) A comparison of finite element and analytic models of acoustic scattering from rough poroelastic interfaces. The Journal of the Acoustical Society of America. 137(4):EL235-EL240.
48. Isakson M, Yarbrough R, Chotiros N (2008) A finite element model for seafloor roughness scattering. In Proceedings of the International Symposium on Underwater Reverberation and Clutter. 173-180.
49. Sapper ED, Hinderliter BR (2013) Computational Tools and Approaches for Design and Control of Coating and Composite Color, Appearance, and Electromagnetic Signature. Coatings 3:59-81.
50. Buxbaum, G. (Ed.). (2008). Industrial inorganic pigments. John Wiley & Sons, New York.
51. Seubert CM, Nichols ME, Frey J, Shtein M, and Thouless MD (2015) The characterization and effects of microstructure on the appearance of platelet–polymer composite coatings. Journal of Materials Science, 51(5):2259-2273.
52. Popovic Z and Popovic BD (2000) Introductory electromagnetics. 382-392, Prentice Hall, Upper Saddler River, New Jersey.

53. Neelakanta PS (1995) Handbook of electromagnetic materials: monolithic and composite versions and their applications. 501-507, CRC press New York, New York.
54. Kasarova SN, Sultanova NG, Ivanov CD, Nikolov ID (2007) Analysis of the dispersion of optical plastic materials. Optical Materials 29:1481-1490.
55. Bartl J, Baranek M (2004) Emissivity of aluminum and its importance for radiometric measurement. Measurement of Physical Quantities 43:31-36.
56. Klein GA, Meyrath T (2010) Industrial color physics. Springer, New York.
57. Möller T (1997) A fast triangle-triangle intersection test. Journal of graphics tools 2:25-30.
58. Bergström D, Powell J, Kaplan AFH (2008) The absorption of light by rough metal surfaces—A three-dimensional ray-tracing analysis. Journal of Applied Physics. 103(10):103515.
59. Garcia N and Stoll E (1984) Monte Carlo calculation for electromagnetic-wave scattering from random rough surfaces. Physical review letters. 52(20):1798.